




**Strong magnetic anisotropy and magnetoelastic coupling in chromium chalcogenide monolayers**Hong-yao Liu (刘洪瑶), Huan Yang (杨欢), and Yujun Zheng (郑雨军)\**School of Physics, Shandong University, Jinan 250100, China*

(Received 26 June 2023; revised 6 January 2024; accepted 12 February 2024; published 27 February 2024)

Two-dimensional (2D) ferromagnets with controllable magnetic anisotropy hold great promise for quantum information processing and sensing. However, realizing large magnetic anisotropy and strong exchange interactions in stable 2D magnetic materials remains a major challenge. Here, we present the identification of strong in-plane magnetic anisotropy in CrSBr-type chromium chalcogenide monolayers. Importantly, the different easy axes of magnetization can be further controlled by applying mechanical strain. The underlying physics are related to the change in the orbital magnetic moment dependent on the lattice. Furthermore, our investigation demonstrates that the optical properties of the Cr<sub>2</sub>SSeBr<sub>2</sub> monolayer are sensitive to the magnetization direction. This study is interesting for achieving new 2D ferromagnets and advancing nanoelectronic devices.

DOI: [10.1103/PhysRevB.109.064425](https://doi.org/10.1103/PhysRevB.109.064425)**I. INTRODUCTION**

With the confirmation of intrinsic magnetism in monolayer Cr<sub>2</sub>Ge<sub>2</sub>Te<sub>6</sub> and CrI<sub>3</sub>, two-dimensional magnetic materials have become an active topic [1,2]. Additionally, 2D magnetic materials in nanoscale spintronic devices have been extensively studied. Under certain conditions, spin liquid and spin glass states may manifest [3,4], which exhibit a variety of physical properties, including magnetoelectricity, magnetism, and magnetocaloric and magnetooptic effects [5–7]. Flexible manipulation of these materials can be achieved through thickness changes, mechanical strain application, external field adjustment, electrolyte charging, and heterojunction assembly [8–10]. Previous studies have demonstrated that the application of a positive gate voltage to trilayer Fe<sub>3</sub>GeTe<sub>2</sub> can successfully increase its Curie temperature ( $T_c$ ) to above 300 K [11]. Furthermore, an electric field can be utilized to transform the magnetic order of double-layer CrI<sub>3</sub> from an antiferromagnetic (AFM) configuration to a ferromagnetic (FM) configuration [12]. These magnetic control methods open up new research opportunities for quantum computing [13], low-dimensional superconductivity [14], and topological magnetism [15].

Magnetic anisotropy is necessary to counteract thermal fluctuations, and previous investigations have demonstrated that many factors could influence the magnetic anisotropy, such as the composition, temperature, external field, interface, or surface charge [16,17]. Additionally, previous studies have been conducted on manipulating the easy axis in 2D FM materials. The direction of the magnetic moment in CrI<sub>3</sub> and Fe<sub>2</sub>GeTe<sub>3</sub> monolayers is perpendicular to the 2D layer, while the Cr<sub>2</sub>Ge<sub>2</sub>Te<sub>6</sub> monolayer has an in-plane easy axis [2].

When the magnetic moment of a CrI<sub>3</sub> monolayer is switched from perpendicular to the plane to parallel to the plane, its electronic structure undergoes a significant transfor-

mation [18]. In addition, tensile strain can reduce the magnetic anisotropy energy (MAE) of the CrI<sub>3</sub> monolayer but not switch the magnetic easy axis to in the plane [19]. Therefore, continuing to understand and explore the mechanism of an adjustable easy axis for two-dimensional magnets is crucial.

Recently, a novel class of 2D FM materials, chromium sulfide halides CrSX ( $X = \text{Cl}, \text{Br}, \text{I}$ ), was reported. These materials exhibit a spin polarization of up to  $3.0 \mu_B$  per unit and a higher  $T_c$  of up to 150 K [20–22]. The monolayer FM order was experimentally confirmed by using second harmonic generation (SHG) to probe the 2D magnetic semiconductor CrSBr, and the  $T_c$  of the CrSBr monolayer was demonstrated to be approximately 146 K. In multilayer form, the FM monolayers are antiferromagnetically coupled, and the Neel temperature of CrSBr decreases as the number of layers increases compared to other 2D magnets [21]. Since the lattice belongs to the  $Pmmn$  space group, its orthorhombic structure exhibits anisotropic characteristics. Thus, the magnetism of the CrSX monolayer with an in-plane easy axis is also anisotropic. In addition, 2D materials with orthosymmetric space group structures tend to be ferroelastic, suggesting that the CrSX monolayer is likely to be a rare 2D multiferroic material exhibiting both ferromagnetism and ferroelasticity. Multiferroic materials are becoming objects of investigation since they have potential applications in functional devices.

The FM coupling of CrSBr-based monolayers, such as CrMoSe<sub>2</sub>Br<sub>2</sub> and CrMoTe<sub>2</sub>Cl<sub>2</sub>, can be significantly enhanced by equivalent alloying [23,24]. Although many studies have been conducted on 2D CrSBr, there is still a lack of research on the physical effects of similar elements on materials and a scarcity of research on substitutional doping of a chalcogen atom into CrSX monolayers. Here, we study the electronic and magnetic properties of five structures after confirming their stability through phonon spectral images by constructing two chromium halide monolayers Cr<sub>2</sub>SSeBr<sub>2</sub> and Cr<sub>2</sub>SSeCl<sub>2</sub>, and a CrSBr/CrSeCl heterostructure. The easy axes of magnetization are all parallel to the two-dimensional plane, and the structures possess strong magnetic anisotropy.

\*yzheng@sdu.edu.cn

Moreover, magnetic and elastic signals can be converted via stress. This demonstrates that chromium-sulfur halide monolayers with excellent magnetically controllable properties are promising for application in quantum information processing and sensing.

## II. COMPUTATIONAL DETAILS

We used the density functional theory (DFT) framework as implemented in the Vienna *ab initio* simulation package (VASP) to perform our first-principles calculations of CrSBr-type monolayers [25], with the projector augmented-wave method (PAW) describing the electron-core interaction [26,27]. The exchange-correlation functional was described by the Perdew, Burke, and Ernzerhof (PBE) formulation of the generalized gradient approximation (GGA) [28]. The plane wave cutoff energy for the self-consistent calculations was taken as 500 eV, and the energy convergence criterion was controlled to  $10^{-6}$  eV. The maximum force allowed on each atom was taken as  $-0.01$  eV/Å. To limit the two-dimensional scale of the material, the thickness of the vacuum layer along the  $z$  axis was set to 20 Å, which is sufficiently large to prevent periodic interactions along the  $c$  direction. Due to the strong correlation effect of the 3d electrons, the GGA usually cannot accurately describe chromium chalcogenide monolayers. To accurately capture the correlation effect of the Cr 3d electrons, the GGA plus Hubbard  $U$  (GGA+ $U$ ) was employed throughout the calculation [29,30], with an effective Hubbard  $U_{\text{eff}}$  of 3 eV, as suggested by Dudarev's Cr- $d$  method [22,31,32]. Possible variations for smaller or higher values of  $U_{\text{eff}}$ , in the range 1 eV – 6 eV, have also been analyzed. Calculations with spin-orbit coupling (SOC) were also conducted to consider the orientation dependence of the spin and orbital magnetic moments [33]. We calculated phonon spectra by using the VASP software package as well as the PHONOPY module [34].

## III. RESULTS AND DISCUSSION

### A. Geometrical structure and stabilities

The materials  $\text{Cr}_2\text{SSeBr}_2$  and  $\text{Cr}_2\text{SSeCl}_2$  are monolayer materials constructed from CrSBr and CrSeCl monolayers. Their structures are similar to that of CrSBr, and these materials are collectively referred to as CrSBr-type chromium chalcogenide monolayers. Constructing heterostructures is an effective means to explore novel properties of materials, and CrSBr and CrSeCl have similar lattice constants. We constructed a CrSBr/CrSeCl heterostructure using the two monolayers for comparison with the monolayers.

Figure 1 shows the crystal lattice structures of the van der Waals (vdW) layered CrSBr-type chromium chalcogenide monolayers in the top and side views. The CrSBr-type monolayer with a  $Pmnm$  orthorhombic space group has a rectangular 2D primitive cell, composed of two buckled planes of Cr and the chalcogen sandwiched between two halogen atomic sheets. The lattice parameters and magnetic moment of each Cr atom ( $M_{\text{Cr}}$ ) of the five materials are listed in Table I. We tested the dependence of  $M_{\text{Cr}}$  on  $U_{\text{eff}}$  (see Table S1 of the Supplemental Material [48]). With increasing  $U_{\text{eff}}$ ,  $M_{\text{Cr}}$  slightly increases. Since there have been some previous

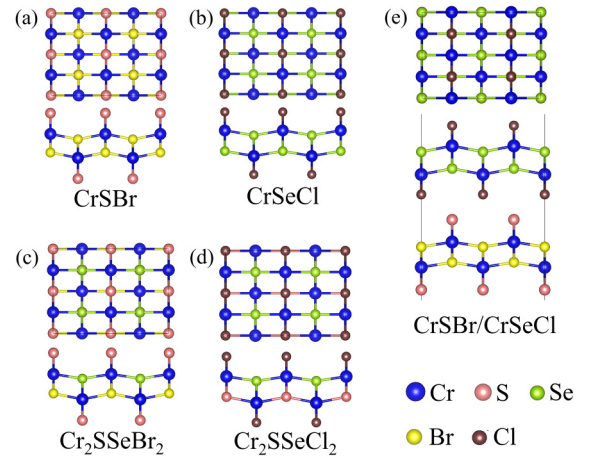


FIG. 1. Structure of chromium chalcogenide monolayers. (a)–(e) Structures of CrSBr, CrSeCl,  $\text{Cr}_2\text{SSeBr}_2$ ,  $\text{Cr}_2\text{SSeCl}_2$ , and the CrSBr/CrSeCl heterostructure.

studies related to 2D CrSBr and CrSeCl with some parameter values listed, we compared the calculated lattice parameters [20,35–38] and magnetic moments [32,39] of the CrSBr and CrSeCl monolayers with those previously reported and found that the results are in great agreement, which proves the accuracy of our calculation method. The optimized structures of the  $\text{Cr}_2\text{SSeBr}_2$  and  $\text{Cr}_2\text{SSeCl}_2$  monolayers have very similar atomic arrangements to those of the CrSBr and CrSeCl monolayers.

To ascertain the magnetic ground state of the chromium chalcogenide monolayers, five potential magnetic configurations, comprising one FM state and four AFM states, were preset using a  $2 \times 2 \times 1$  supercell, as depicted in Fig. S1 of the Supplemental Material [48]. The energy results for the various magnetic ground states are tabulated in Table II. All the systems have the lowest system energy in the FM state and thus exhibit the FM state. To confirm the stability of the lattice dynamics, we calculated the phonon spectra of the CrSBr-type chromium chalcogenide monolayers (the detailed figures can be found in Fig. S2 of the Supplemental Material [48]). The results show that there is no virtual frequency in the first Brillouin zone, which guarantees the dynamic stability of the chromium chalcogenide monolayers and the heterostructure they constitute.

### B. Electronic properties

We calculated the electronic properties of the CrSBr monolayer with and without spin polarization (see Fig. S3 and Fig. S4 of the Supplemental Material [48]). Notably,

TABLE I. Lattice constant and magnetic moments of Cr atoms ( $M_{\text{Cr}}$ ) of the chromium chalcogenide monolayers.

|                        | CrSBr | CrSeCl | $\text{Cr}_2\text{SSeBr}_2$ | $\text{Cr}_2\text{SSeCl}_2$ | CrSBr/CrSeCl |
|------------------------|-------|--------|-----------------------------|-----------------------------|--------------|
| $a(\text{Å})$          | 4.76  | 5.07   | 4.92                        | 4.94                        | 4.92         |
| $b(\text{Å})$          | 3.56  | 3.54   | 3.60                        | 3.50                        | 3.55         |
| $M_{\text{Cr}}(\mu_B)$ | 3.24  | 3.31   | 3.33                        | 3.30                        | 3.21         |

TABLE II. Relative total energies  $\Delta E$  (meV/unit cell) of the chromium chalcogenide monolayers in different magnetic states.

| State | CrSBr | CrSeCl | Cr <sub>2</sub> SSeBr <sub>2</sub> | Cr <sub>2</sub> SSeCl <sub>2</sub> | CrSBr/CrSeCl |
|-------|-------|--------|------------------------------------|------------------------------------|--------------|
| FM    | 0     | 0      | 0                                  | 0                                  | 0            |
| AM1   | 113.9 | 114.8  | 142.1                              | 118.7                              | 212.0        |
| AM2   | 99.2  | 282.5  | 157.0                              | 87.1                               | 439.0        |
| AM3   | 368.2 | 442.2  | 347.9                              | 87.2                               | 437          |

the CrSBr, Cr<sub>2</sub>SSeBr<sub>2</sub>, and Cr<sub>2</sub>SSeCl<sub>2</sub> monolayers and the CrSBr/CrSeCl heterostructure are semiconductors, while the CrSeCl system behaves as a metal, without taking SOC into account. The direct bandgaps of the semiconductor systems are 0.67 eV, 0.30 eV, 0.37 eV, and 0.14 eV. In addition, we evaluated the gap values of these four materials under different  $U_{\text{eff}}$  values (the detailed results are listed in Table S2 of the Supplemental Material [48]). Within the range of 1 ~ 6 eV of  $U_{\text{eff}}$ , the bandgaps of Cr<sub>2</sub>SSeBr<sub>2</sub> and Cr<sub>2</sub>SSeCl<sub>2</sub> monolayers and the CrSBr/CrSeCl heterostructure decreases as  $U_{\text{eff}}$  increases. We speculate that the reason for this phenomenon is the combined influence of coulomb interaction and magnetism.

The valence band maximum (VBM) and conduction band minimum (CBM) are located at the  $\Gamma$  point, and the band structure is consistent with that of previous reports. Direct bandgap semiconductors are more suitable for optoelectronic applications and field-effect transistors, as electrons in the CBM can be directly excited to the VBM without involving phonon interactions.

According to the density of states diagram, the CBM of the semiconductors is mainly composed of the  $P_y$  orbital of the halogen, and the VBM is mainly contributed by the Cr atom, with the  $dz^2$  and  $dx^2-dy^2$  orbitals being the most prominent (the detailed figures are illustrated in Fig. S5 of the

Supplemental Material [48]). For the CrSeCl material, the  $p$  orbital crosses the Fermi level, resulting in a metallic ground state. Since the Cr atom is a 3d element, the calculation was performed with SOC turned on. The results show that for the four semiconductor materials, SOC leads to narrowing of the bandgap, ranging from 0.2 ~ 0.4 eV, while the direct bandgap nature remains unchanged. Interestingly, for the CrSeCl monolayer, the SOC opens a weak bandgap of 16 meV, resulting in rearrangement of the electronic structure.

### C. Magnetic anisotropy and strain tuning

The MAE originating from the SOC effect is an important parameter for ensuring stability of the long-range magnetic order [35,40]. To confirm the magnetic anisotropy in these monolayers, we calculate the energy change of the FM materials for different orientations of the magnetic moment by rotating its direction.

The results of Fig. 2 reveal the angular dependence of the MAE in the  $xoy$ ,  $yo\bar{z}$ , and  $zox$  planes, which is anisotropic and preferentially dependent on the magnetic orientation. The easy axes of the four monolayers are along the (010) direction, while the easy axis of the CrSBr/CrSeCl heterostructure is along the (100) direction. The CrSeCl material has the greatest MAE (142.5  $\mu\text{eV}/\text{Cr}$  atom). In addition, Cr<sub>2</sub>SSeBr<sub>2</sub> and the CrSBr/CrSeCl heterostructure exhibit satisfactory MAEs of 105 and 52.5  $\mu\text{eV}/\text{Cr}$ , respectively. Our calculated MAEs are greater than those enumerated for some 2D FM materials, such as VOBr<sub>2</sub> (14.4  $\mu\text{eV}/\text{V}$  atom), VOCl<sub>2</sub> (16.6  $\mu\text{eV}/\text{V}$  atom) [41], and CrGeTe<sub>3</sub> (20  $\mu\text{eV}/\text{Cr}$  atom) [42]. Theoretically, the larger the MAE is, the more resistant the material is to disturbance of the FM order caused by thermal fluctuations at a specific temperature. The above results are based on the case of  $U_{\text{eff}} = 3$  eV, where  $U_{\text{eff}} = 3$  eV gives the best agreement in case of magnetic moment magnitudes so it is

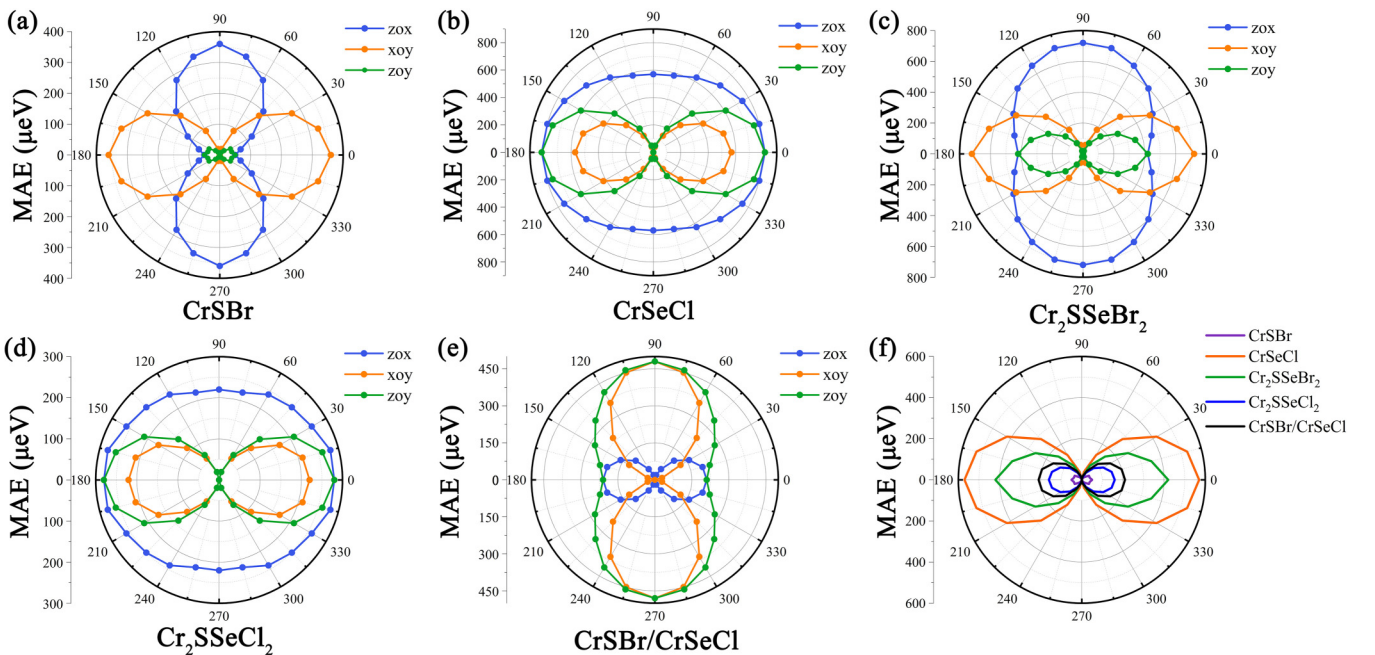
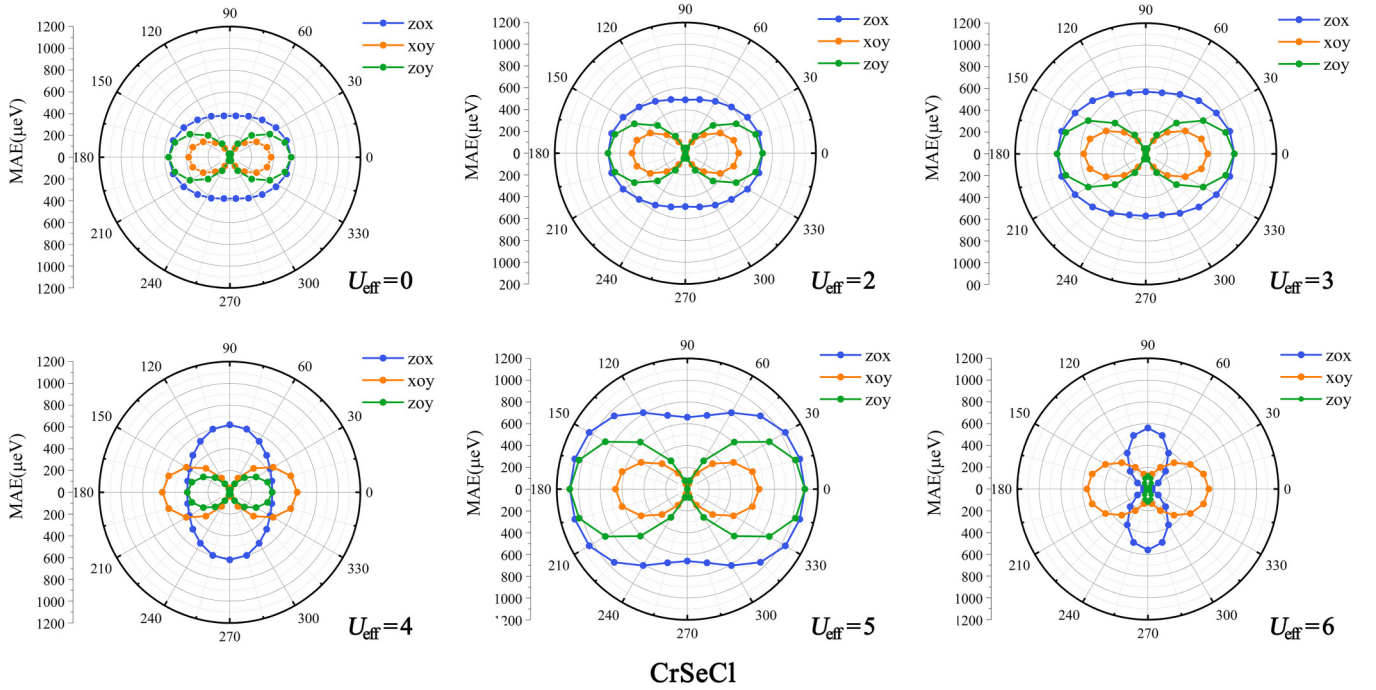


FIG. 2. Magnetic anisotropy of the chromium chalcogenide monolayers.

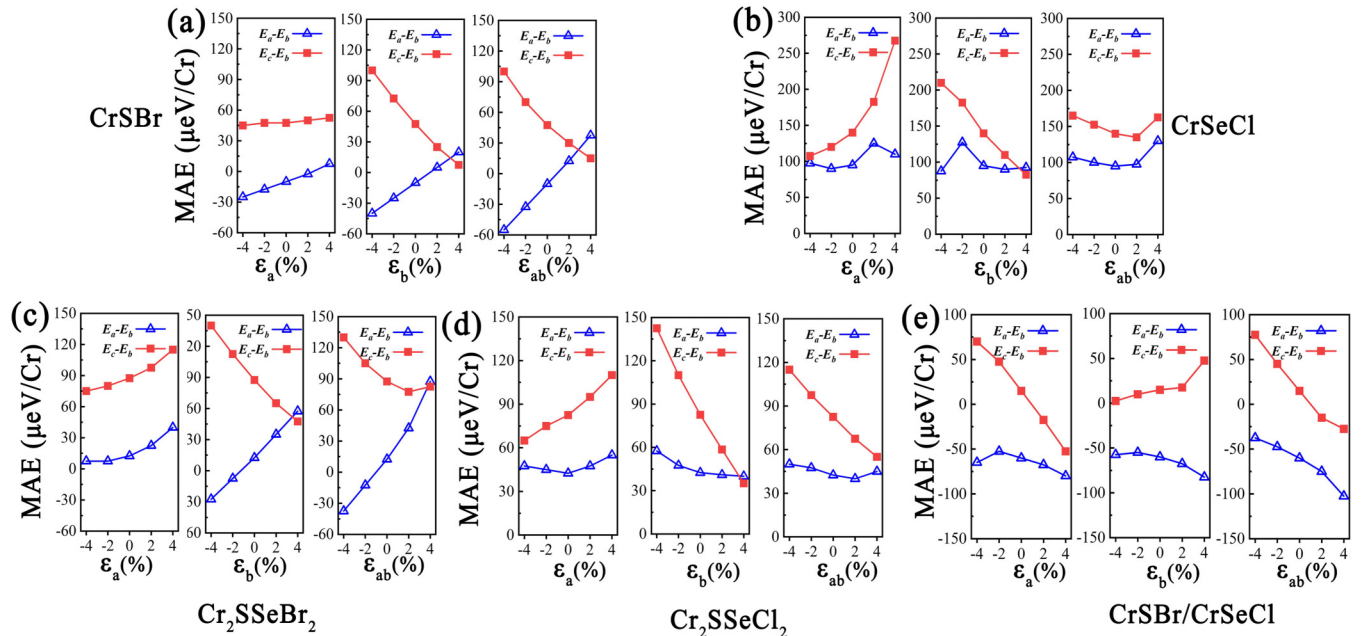


FIG. 3. MAEs of the CrSeCl monolayer under different Hubbard  $U_{\text{eff}}$  values.

used also to predict MAE. We also considered the MAEs of the five materials under different  $U_{\text{eff}}$  values, as displayed in Fig. 3 and Figs. S6–S9 of the Supplemental Material [48]. The MAE responses to  $U_{\text{eff}}$  for several materials present different trends. When the  $U_{\text{eff}}$  of the CrSeCl monolayer reaches 6 eV, the easy axis changes from in plane to out of plane.

Low-dimensional materials often exhibit sensitive responses to external stimuli, enabling their electronic properties or magnetism to be accordingly tuned. Strain tuning

is a versatile method for tuning the electronic properties of 2D layered structures. Since the long-range magnetic order is mainly driven by exchange interactions and is determined by the distance between adjacent magnetic ions or the distance between these ions and ligand atoms (bond angle) [19,43], the magnetic anisotropy is related to the coordination field, SOC, and orbital magnetic moment, which are all closely related to the lattice. By altering the bond angles and distances between atoms, the interaction between them can be

FIG. 4. MAEs of the chromium chalcogenide materials under a biaxial strain (along the  $a$  and  $b$  axis) or a uniaxial strain (along the  $a$  or  $b$  axis).

modified, thereby resulting in changes in the electronic properties. The FM order can be switched on and off via strain-induced control [44]. In double-layer  $\text{CrI}_3$ , a tensile stress stabilizes the AFM state of the material, whereas a compressive stress causes the material to transition into an FM state [45]. This is due to the induced displacement between the layers, which alters the magnetic order. Here, we show that the easy axis in CrSBr-type chromium chalcogenide monolayers can also be manipulated by elastic strain.

In our calculations, biaxial strain  $\varepsilon$  is defined as  $\varepsilon = (a - a_0)/a_0$ , with  $a$  and  $a_0$  representing the lattice constants of 2D materials under strained and unstrained conditions, respectively. Our results on the strain effect on the CrSBr monolayer reveal that the application of a 4% uniaxial strain in the  $a$  direction causes the energy difference between  $E_a$  and  $E_b$  to transition from negative to positive and the easy magnetization axis to shift from the original  $a$  axis to the  $b$  axis, as shown in Fig. 4. Additionally, when a 2% or 4% tensile strain is applied in the  $b$  direction or a 2% or 4% biaxial strain is concurrently applied in the  $a$  and  $b$  directions, the same outcome is observed. The situation for the  $\text{Cr}_2\text{SSeBr}_2$  monolayer is exactly the opposite to that for CrSBr. When a compressive strain of 2% or 4% is applied in the  $b$  direction or a biaxial compressive strain of 2% or 4% is applied in the  $a$  and  $b$  directions, the easy magnetization axis of  $\text{Cr}_2\text{SSeBr}_2$  shifts from the  $b$  axis to the  $a$  axis. Elastic deformation does not directly alter the magnetic easy axes of CrSeCl,  $\text{Cr}_2\text{SSeCl}_2$ , or the CrSBr/CrSeCl heterostructure, but certain degrees of tensile and compressive strain can enhance the MAE. For example, when a 2% tensile strain is applied along the  $a$  axis of the CrSeCl monolayer, the difference between  $E_a$  and  $E_b$  increases, but remains positive. For the CrSBr/CrSeCl heterostructure, the influence of a biaxial strain along the  $a$  and  $b$  axes on the MAE shows regular changes: when a compressive strain is applied, the MAE decreases with increasing strain, and when a tensile strain is applied, the MAE increases with increasing strain.

#### D. Magneto-optical response and magnetoelectric coupling properties

The chalcogenide monolayer structure with triaxial magnetic anisotropy is expected to effectively couple magnetic effects in response to visible light. To better understand the magneto-optical response of the five materials, we calculated the light absorption coefficient  $\alpha(\omega)$  for different magnetic moment directions. In this part,  $\alpha(\omega)$  is obtained from the real part  $\varepsilon_1(\omega)$  and imaginary part  $\varepsilon_2(\omega)$  of the dielectric function via [46]

$$\alpha(\omega) = \sqrt{2} \frac{\omega}{c} \sqrt{\sqrt{\varepsilon_1^2(\omega) + \varepsilon_2^2(\omega)} - \varepsilon_1(\omega)}. \quad (1)$$

The dielectric function  $\varepsilon_2(\omega)$  can be obtained by DFT using

$$\varepsilon_2(\omega) = \frac{4\pi^2}{m^2\omega^2} \sum_{c,v} \int_{\text{BZ}} \frac{2}{(2\pi)^3} |M_{c,v}(k)|^2 \delta(\varepsilon_{ck} - \varepsilon_{vk} - \hbar\omega) d^3k, \quad (2)$$

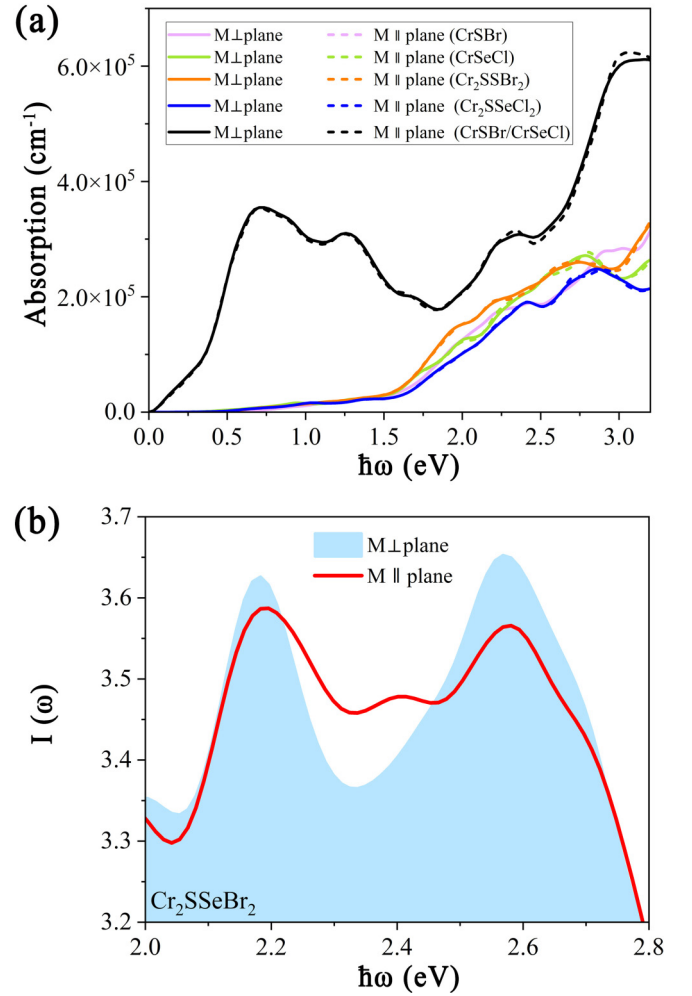


FIG. 5. (a) Variation in the optical absorption coefficient with magnetic moment rotation in the chromium chalcogenide monolayers. (b) Relationship between the magnetic moment arrangement and the imaginary part of the dielectric functional in  $\text{Cr}_2\text{SSeBr}_2$ .

where  $|M_{c,v}(k)|^2$  represents the momentum matrix element. The conduction and valence band states are represented by  $c$  and  $v$ , respectively. The real part  $\varepsilon_1$  is derived from the imaginary part by employing the Kramers-Kronig transformation [47].

The relationship between the light absorption coefficient and photon energy is shown in panel (a) of Fig. 5 when the magnetic moment is along the in-plane or out-of-plane direction, with the solid line indicating a perpendicular orientation and the dotted line indicating a parallel orientation. Among the 2D chalcogenide materials, the CrSBr/CrSeCl heterostructure has the most significant light absorption range, with absorption in both the infrared and visible light regions. The first absorption peak appears in the low-frequency range up to  $3.8 \times 10^5 \text{ cm}^{-1}$ , which may be directly related to the interband transition. In the visible light region, the light absorption coefficient reaches  $6 \times 10^5 \text{ cm}^{-1}$ . Panel (b) of Fig. 5 shows how the imaginary part  $\varepsilon_2(\omega)$  of the dielectric function of  $\text{Cr}_2\text{SSeBr}_2$  is affected by the magnetic moment. We calculated  $\varepsilon_2(\omega)$  for the magnetization in two directions in monolayer  $\text{Cr}_2\text{SSeBr}_2$ . For the in-plane magnetization,  $\varepsilon_2(\omega)$

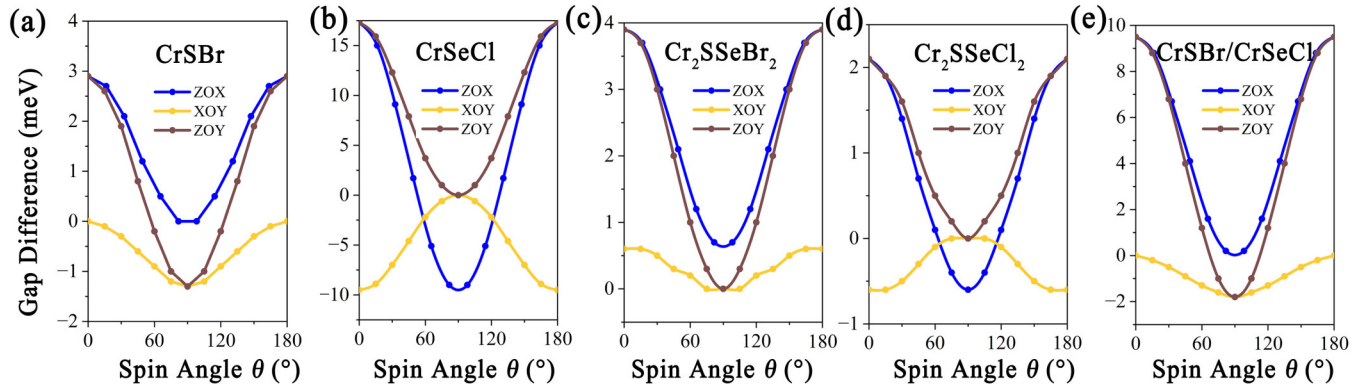


FIG. 6. Variation in the bandgaps of the chromium chalcogenide monolayers with magnetic moment rotation. The different colored lines indicate different planes, as shown in the figure.

exhibits a faint peak in the visible region at approximately 2.4 eV. However, for the out-of-plane magnetization, this does not occur. We also calculated  $\varepsilon_2(\omega)$  for different magnetic moment arrangements in the case of  $U_{\text{eff}} = 6$  eV (see Fig. S10 in the Supplemental Material [48].) At such a large  $U_{\text{eff}}$ , the trend of  $\varepsilon_2(\omega)$  is significantly affected.

Furthermore, in CrSBr-type chromium chalcogenide monolayers, the electronic structural properties can be controlled by the magnetoelectric coupling effect. As illustrated in Fig. 6, when the polarization direction is rotated, the bandgap of these monolayers exhibits a regular change. Specifically, when the magnetic moment is rotated away from the easy axis direction in the plane, the  $\text{Cr}_2\text{SSeBr}_2$  bandgap decreases with increasing rotation angle, as depicted by the yellow curve in Fig. 6. However, the bandgaps of the other four 2D materials increase with the rotation of the magnetic moment. Consequently, by manipulating the polarization direction, the electronic properties can be tuned as expected, which may lead to potential applications such as nanoswitches and rectifying junctions in spintronic devices.

#### IV. SUMMARY

In this work, we conducted a systematic investigation of the structures, electronic properties, and magnetic interactions of five chromium chalcogenide monolayers in

the FM state, considering the regulation of the material magnetism by strain. We revealed that the in-plane magnetocrystalline anisotropy of chromium halide monolayers can be effectively enhanced by tuning the external force, while the easy magnetization axis can also be tuned by strain. In addition, band structure analysis revealed that the CrSeCl monolayer exhibited opening of a bandgap of approximately 16 meV after considering SOC. We further observed that the electronic and optical properties change with the magnetic axis, demonstrating the interplay of magnetism and electricity, magnetism and force, and magnetism and optics, which can potentially be applied to highly integrated optoelectronic magnetic devices. Our findings may thus inspire further experimental studies on chromium chalcogenides, thereby expanding the family of magnetic materials. After that, consideration of new stable 2D magnetic chromium chalcogenides and other types of 2D materials to form heterostructures may be possible, which may provide an ideal platform for the study of novel topological quantum states, superconductivity, and quantum information processing.

#### ACKNOWLEDGMENT

This work was supported by the National Natural Science Foundation of China (Grants No. 12234013 and No. 12174221).

- [1] C. Gong, L. Li, Z. Li, H. Ji, A. Stern, Y. Xia, T. Cao, W. Bao, C. Wang, Y. Wang *et al.*, *Nature (London)* **546**, 265 (2017).
- [2] B. Huang, G. Clark, E. Navarro-Moratalla, D. R. Klein, R. Cheng, K. L. Seyler, D. Zhong, E. Schmidgall, M. A. McGuire, D. H. Cobden *et al.*, *Nature (London)* **546**, 270 (2017).
- [3] E. Maniv, R. A. Murphy, S. C. Haley, S. Doyle, C. John, A. Maniv, S. K. Ramakrishna, Y.-L. Tang, P. Ercius, R. Ramesh *et al.*, *Nat. Phys.* **17**, 525 (2021).
- [4] L. Savary and L. Balents, *Rep. Prog. Phys.* **80**, 016502 (2017).
- [5] F. Fan, D. Zhao, Z. Tan, Y. Ji, J. Cheng, and S. Chang, *Adv. Opt. Mater.* **9**, 2101097 (2021).
- [6] A. Qaiumzadeh, H. Skarsvåg, C. Holmqvist, and A. Brataas, *Phys. Rev. Lett.* **118**, 137201 (2017).
- [7] X. Yang, X. Zhou, W. Feng, and Y. Yao, *Phys. Rev. B* **103**, 024436 (2021).
- [8] F. Hellman, A. Hoffmann, Y. Tserkovnyak, G. S. D. Beach, E. E. Fullerton, C. Leighton, A. H. MacDonald, D. C. Ralph, D. A. Arena, H. A. Durr, P. Fischer, J. Grollier, J. P. Heremans, T. Jungwirth, A. V. Kimel, B. Koopmans, I. N. Krivorotov, S. J. May, A. K. Petford-Long, J. M. Rondinelli, N. Samarth, I. K. Schuller, A. N. Slavin, M. D. Stiles, O. Tchernyshyov, A. Thiaville, B. L. Zink, *Rev. Mod. Phys.* **89**, 025006 (2017).
- [9] K. L. Seyler, D. Zhong, D. R. Klein, S. Gao, X. Zhang, B. Huang, E. Navarro-Moratalla, L. Yang, D. H. Cobden, M. A. McGuire *et al.*, *Nat. Phys.* **14**, 277 (2018).

- [10] Y. Gao, Q. Liu, X. Jiang, and J. Zhao, *Appl. Phys. Lett.* **121**, 162402 (2022).
- [11] Y. Deng, Y. Yu, Y. Song, J. Zhang, N. Z. Wang, Z. Sun, Y. Yi, Y. Z. Wu, S. Wu, J. Zhu *et al.*, *Nature (London)* **563**, 94 (2018).
- [12] B. Huang, G. Clark, D. R. Klein, D. MacNeill, E. Navarro-Moratalla, K. L. Seyler, N. Wilson, M. A. McGuire, D. H. Cobden, D. Xiao *et al.*, *Nat. Nanotechnol.* **13**, 544 (2018).
- [13] D. Lachance-Quirion, Y. Tabuchi, A. Glorpe, K. Usami, and Y. Nakamura, *Appl. Phys. Express* **12**, 070101 (2019).
- [14] A. Brataas, B. van Wees, O. Klein, G. de Loubens, and M. Viret, *Phys. Rep.* **885**, 1 (2020).
- [15] L. Šmejkal, Y. Mokrousov, B. Yan, and A. H. MacDonald, *Nat. Phys.* **14**, 242 (2018).
- [16] W. Weber, A. Bischof, R. Allenspach, C. Wüsch, C. H. Back, and D. Pescia, *Phys. Rev. Lett.* **76**, 3424 (1996).
- [17] M. Farle, *Rep. Prog. Phys.* **61**, 755 (1998).
- [18] Z. Fei, B. Huang, P. Malinowski, W. Wang, T. Song, J. Sanchez, W. Yao, D. Xiao, X. Zhu, A. F. May *et al.*, *Nat. Mater.* **17**, 778 (2018).
- [19] L. Webster and J.-A. Yan, *Phys. Rev. B* **98**, 144411 (2018).
- [20] C. Wang, X. Zhou, L. Zhou, N.-H. Tong, Z.-Y. Lu, and W. Ji, *Sci. Bull.* **64**, 293 (2019).
- [21] K. Lee, A. H. Dismukes, E. J. Telford, R. A. Wisconsin, J. Wang, X. Xu, C. Nuckolls, C. R. Dean, X. Roy, and X. Zhu, *Nano Lett.* **21**, 3511 (2021).
- [22] H. Wang, J. Qi, and X. Qian, *Appl. Phys. Lett.* **117**, 083102 (2020).
- [23] S. Chen, F. Wu, Q. Li, H. Sun, J. Ding, C. Huang, and E. Kan, *Nanoscale* **12**, 15670 (2020).
- [24] Y. Zheng, Y. Wang, Z. Wang, X. Li, Y. Liang, C. Huang, and F. Wu, *J. Phys. Chem. C* **126**, 17390 (2022).
- [25] G. Kresse and J. Hafner, *Phys. Rev. B* **47**, 558 (1993).
- [26] P. E. Blöchl, *Phys. Rev. B* **50**, 17953 (1994).
- [27] G. Kresse and D. Joubert, *Phys. Rev. B* **59**, 1758 (1999).
- [28] J. P. Perdew, K. Burke, and M. Ernzerhof, *Phys. Rev. Lett.* **77**, 3865 (1996).
- [29] S. L. Dudarev, G. A. Botton, S. Y. Savrasov, C. J. Humphreys, and A. P. Sutton, *Phys. Rev. B* **57**, 1505 (1998).
- [30] M. Cococcioni and S. de Gironcoli, *Phys. Rev. B* **71**, 035105 (2005).
- [31] K. Yang, G. Wang, L. Liu, D. Lu, and H. Wu, *Phys. Rev. B* **104**, 144416 (2021).
- [32] M. Li and B. Zhou, *J. Phys. Chem. C* **127**, 22378 (2023).
- [33] D. Hobbs, G. Kresse, and J. Hafner, *Phys. Rev. B* **62**, 11556 (2000).
- [34] A. Togo and I. Tanaka, *Scr. Mater.* **108**, 1 (2015).
- [35] Y. Guo, Y. Zhang, S. Yuan, B. Wang, and J. Wang, *Nanoscale* **10**, 18036 (2018).
- [36] Z. Jiang, P. Wang, J. Xing, X. Jiang, and J. Zhao, *ACS Appl. Mater. Interfaces* **10**, 39032 (2018).
- [37] C. Hou, X. Wang, Y. Sun, Y. Lu, and J. Ni, *J. Phys. Chem. C* **127**, 22833 (2023).
- [38] S. A. López-Paz, Z. Guguchia, V. Y. Pomjakushin, C. Witteveen, A. Cervellino, H. Luetkens, N. Casati, A. F. Morpurgo, and F. O. von Rohr, *Nat. Commun.* **13**, 4745 (2022).
- [39] J. Xiao, D. Legut, W. Luo, H. Guo, X. Liu, R. Zhang, and Q. Zhang, *Phys. Rev. B* **101**, 014431 (2020).
- [40] X. Wang, R. Wu, D.-S. Wang, and A. J. Freeman, *Phys. Rev. B* **54**, 61 (1996).
- [41] H. Ai, X. Song, S. Qi, W. Li, and M. Zhao, *Nanoscale* **11**, 1103 (2019).
- [42] C. Xu, J. Feng, H. Xiang, and L. Bellaiche, *npj Comput. Mater.* **4**, 57 (2018).
- [43] X. Hu, Y. Zhao, X. Shen, A. V. Krasheninnikov, Z. Chen, and L. Sun, *ACS Appl. Mater. Interfaces* **12**, 26367 (2020).
- [44] H. Y. Lv, W. J. Lu, D. F. Shao, Y. Liu, and Y. P. Sun, *Phys. Rev. B* **92**, 214419 (2015).
- [45] A. M. León, J. W. González, J. Mejía-López, F. C. de Lima, and E. S. Morell, *2D Mater.* **7**, 035008 (2020).
- [46] X. Huang, T. R. Paudel, S. Dong, and E. Y. Tsymbal, *Phys. Rev. B* **92**, 125201 (2015).
- [47] M. Gajdoš, K. Hummer, G. Kresse, J. Furthmüller, and F. Bechstedt, *Phys. Rev. B* **73**, 045112 (2006).
- [48] See Supplemental Material at <http://link.aps.org/supplemental/10.1103/PhysRevB.109.064425> for details of magnetic moment arrangement, phonon spectrum, electronic properties and magnetic anisotropy.